Available online at www.sciencedirect.com
SCIENCE DIRECT®
International Journal of Heat and Mass Transfer 48 (2005) 4287–4299
International Journal of HEAT and MASS TRANSFER
www.elsevier.com/locate/ijhmt

Visualization study of pool boiling from thin confined enhanced structures

Camil-Daniel Ghiu, Yogendra K. Joshi *

G.W. Woodruff School of Mechanical Engineering, Georgia Institute of Technology, Atlanta, Georgia 30332, United States

Received 13 April 2005; received in revised form 27 May 2005

Abstract

A visualization study of pool boiling at atmospheric pressure from top-covered enhanced structures was conducted for a dielectric fluorocarbon liquid (PF 5060). The single layer enhanced structures studied were fabricated in copper and quartz, had an overall size of 10 mm × 10 mm and were 1 mm thick. The parameters investigated in this study were the heat flux (in the range of 1–11 W/cm^2 for copper and 1–4 W/cm^2 for quartz) and the width of the microchannels (65–360 μm). A high-speed camera (maximum frame rate 1000 f/s at full resolution) with attached magnifying lens allowed precise observation of the evaporation process in the bottom and top channels. The heat transfer performance of the enhanced structures was found to depend weakly on the channel width. The internal evaporation has a significant contribution to the total heat dissipation, especially at low heat fluxes.

1. Introduction

As the heat dissipated by the newer generation of electronic chips continues to increase, existing air cooling hardware has became too large to meet the overall electronic system size constraints in many applications. For these applications the primary heat sources (chips) are located in a densely packed zone, requiring the need to remove heat from tight spaces. Further exacerbating the spatial constraint is the trend to move away from two-dimensional chip architectures that have so far received the attention of the thermal community, to three-dimensional electronics. The cooling device studied in the present work has a potential to meet such emerging needs. The device is a thin flat structure equipped with a network of interconnected microchannels. The network is composed of two sets of parallel microchannels, one provided on the top side of the device, and the other on the bottom, as seen in Fig. 1(a). These two sets of channels are orthogonal to each other and have interconnecting ports (internal pores) at the intersections (Fig. 1(c)). The microchannel net provides a large surface area in a given volume. This increases the probability of bubble nucleation, and once a bubble is formed at a local spot in a channel, vapor can spread throughout the channel, as well as to other channels through interconnections. This produces the benefit of negating the temperature overshoot at boiling inception.

The steady-state performance of the microchannel net depends on how effectively the large internal surface area can participate in evaporative heat transfer. In an ideal situation, a large percentage of the channel area

* Corresponding author. Tel.: +1 40 4 385 2810; fax: +1 40 4 894 8496.
E-mail address: yogendra.joshi@me.gatech.edu (Y.K. Joshi).

0017-9310/$ - see front matter © 2005 Elsevier Ltd. All rights reserved.
doi:10.1016/j.ijheatmasstransfer.2005.05.024

Nomenclature

A	area of the structure (projected) (m^2)	q''	heat flux based on projected surface area (W/cm^2)
A_b	area available for boiling (m^2)	q	heat rate (W)
A_c	area available for conduction (m^2)	T_{sat}	saturation temperature of liquid, PF 5060 (K)
A_w	structure wetted area (m^2)	T_{wall}	temperature at base of enhanced structure (K)
H_t	channel depth (m)	W_t	channel width (m)
k	thermal conductivity (W/m K)	ΔT_w	wall superheat (K)
k_{eff}	effective thermal conductivity (W/m K)		
L	overall length of the structure (m)		
N	number of channels		
P_t	channel pitch (m)		

is covered by thin liquid films; being known that the evaporation of such films yields a high heat transfer coefficient. Realization of such two-phase heat transfer mode depends on the fluid dynamics working throughout the channel net. The key components of dynamics are ejection of bubbles from the side pores to the open space and resulting dynamic pressure variations inside the channels that induce liquid influx to the channels. In an ideal cycle these key components work in concert, and a proper amount of liquid is introduced and spread in the channels. If the liquid is locally in short supply, a large percentage of the channel wall is dried up. Excess amount of liquid does not help heat transfer in the channels either.

In earlier publications Nakayama et al. [1–3] studied the heat transfer from different types of enhanced structures, and coined the terms "suction-evaporation mode" for the ideal cycle, "dried up mode" for the state of inadequate liquid supply, and "flooded mode" for that of excessive liquid supply. The parameters that determine the internal two-phase mode are many, as will be listed in the next section. Our focus in the present paper is on the channel width and the heat flux. By visualization of two-phase flow inside the microchannel net we attempt to understand the various operating flow regimes.

The enhancement structures studied in earlier publications [1–5] are composed of an array of microchannels covered by circular pores forming a re-entrant type cavity. Nakayama et al. [1] were the first to perform a visualization study on a porous structure. Their single-tunnel, horizontally orientated apparatus permitted side observation of the internal evaporation. Tunnel heights were varied between 0.5 and 1 mm, with the width held fixed at 1 mm. The visualization study suggested that vaporization inside the tunnel played an important role in enhancing heat transfer.

Arshad and Thome [4] employed a brass block having triangular, rectangular and circular cross-section grooves on its top surface. A thin copper sheet having discrete pores covered the grooves. They observed the ends of tunnels and concluded that the evaporation of the thin liquid film is the main boiling mechanism for the structured surfaces. Chien and Webb [5] conducted visualizations using an enhanced tubular surface having rectangular cross-section sub-surface tunnels and surface pores. The experiments were conducted in horizontal and vertical orientations using saturated and sub-cooled methanol at atmospheric pressure. For the vertical tube, they found that all the tunnels were vapor filled except for liquid menisci in the corners. This also held true for the horizontal tube at high heat flux. The authors also concluded that the principal boiling mechanism for the structured surfaces is evaporation of liquid menisci in the tunnel corners.

The above-mentioned investigations treated only the unconfined case, however. Nakayama et al. [6] were the first to study boiling from enhanced structures in a fully confined configuration. They sandwiched an enhanced structure of the present form (Fig. 1(a)) between two chip heaters in vertical position. The single layer enhanced structure served to model one sub-surface layer of a stacked porous stud. The boiling curve obtained with the structure produced the heat transfer coefficient applied to the open surface of the stud. The mechanism of boiling from fully confined enhanced structures was not revealed since no visualizations were performed.

Ghiu et al. [7] performed a visualization study of pool boiling from transparent quartz structures of the present form. The channel widths studied were 0.090 mm and 0.285 mm. The top of the structures was covered with a quartz plate having the same overall dimensions (10 mm × 10 mm × 1 mm). Three boiling regimes were identified: *slug formation* (in either top or bottom channels), *slug migration* between the top and bottom channels and *slug predominance* (most of channels vapor filled). Their study did not contain data for structures made of higher thermal conductivity materials (copper, silicon).

Evaporation of and convection to the liquid can occur both on the exterior surfaces of an enhanced boiling structure or inside its passageways. A key objective of the present work is to assess the importance of internal

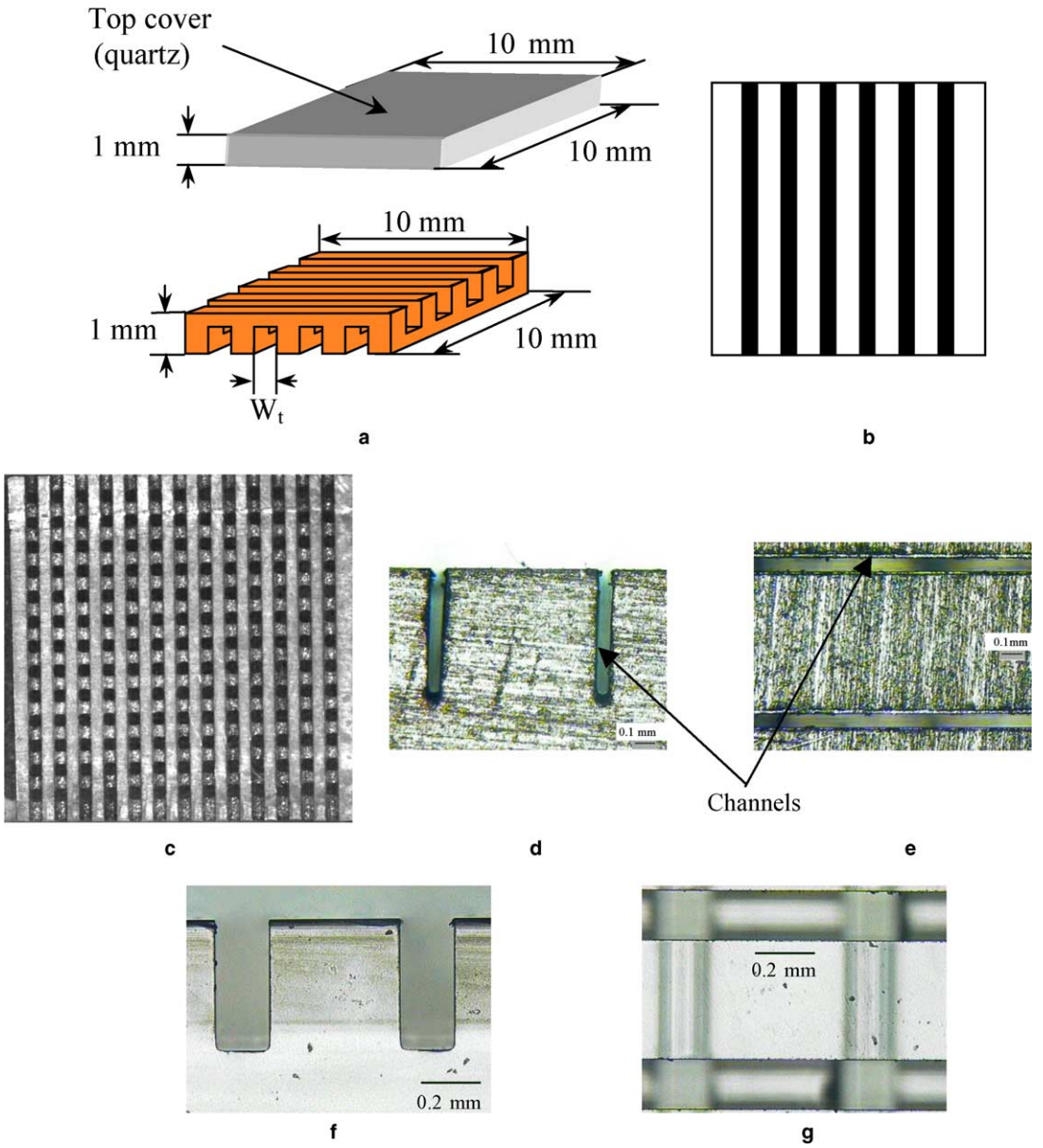

Fig. 1. Enhanced structures used in this study, shown with the confining plate: (a) sketch illustrating microchannels on the top and bottom faces; (b) sketch of the top surface of the heater; (c) pore formation at the intersection of microchannels. Top view of structure C-0.360-0.7 is shown; (d) magnified (50×) picture of the structure C-0.065-0.7, lateral view; (e) magnified (50×) picture of the structure C-0.065-0.7, top view; (f) magnified (50×) picture of the structure Q-0.200-0.7, lateral view and (g) magnified (50×) picture of the structure Q-0.200-0.7, top view.

evaporation among the heat transfer mechanisms responsible for the enhancement of boiling brought about by the structured surfaces. For this purpose the top surface was completely closed with an insulating transparent plate made of quartz. Therefore, for this particular configuration, the primary heat transfer mechanisms are conduction within the structure, internal evaporation, internal convection (superheating of the liquid drawn into and driven out of the structure by the bubble pumping action) and external convection from the fluid exposed sides.

A better understanding of the boiling phenomena from the enhanced structures can be achieved by employing transparent quartz structures. Visualization of boiling within a single-layer structure whose top surface is blocked with a transparent plate provides a

qualitative understanding of boiling from sub-surface layers. This situation can occur in applications when there is complete confinement in the vertical direction, for example in next generation three-dimensionally stacked layers of powered electronic chips [8]. Moreover, the single-layered structures studied here are often used in a stacked configuration to enhance the overall thermal performance. In this case, the bonding between individual layers may require the presence of a thin metallic foil (for instance, gold; see Ramaswamy [9]). Hence the completely covered top situation may be encountered in many practical implementations. The insulated condition is chosen to provide a well-controlled thermal boundary. There is virtually no data on the boiling performance of the single-layered enhanced structures in such closed-top configuration.

In light of the above, the objectives of the present study are to

(i) Investigate the thermal performance of the enhanced structures in the limiting case of insulated top confinement.
(ii) Assess the effect of channel width W_t on the thermal performance. It is expected that this geometric parameter will have a large influence on the boiling phenomena. For a fixed channel pitch P_t, the wider the channel, the larger the area available for boiling heat transfer and the smaller the area exposed to conduction.
(iii) Understand the boiling phenomena, as well as identify the boiling regimes, that might establish from the enhanced structures with insulated top, through high speed visualizations.

2. Enhanced structures

A schematic diagram and optical micrographs of the enhanced structure are presented in Fig. 1. The single layer structures were fabricated in both copper and quartz, had an overall size of 10 mm × 10 mm and were 1 mm thick. Their geometrical parameters are summarized in Table 1. The term (A_w/A) designates the ratio between the total wetted area of the structure and the base projected area. The entry (A_c/A) signifies the fraction of the base projected area in contact with the top cover. The copper structures with small channel widths (C-0.065-0.7, C-0.085-0.7 and C-0.105-0.7) and all the quartz structures were manufactured by employing an automated wafer dicing saw. The cutting element consisted of nickel or resinoid blades (having diamond particles embedded at the periphery) rotating at 30,000 rpm. A row of parallel microchannels was cut on the bottom surface. The top surface also had parallel microchannels aligned 90° to those on the bottom surface (Fig. 1(a)). Since the depth of the microchannels (0.6 mm) was more than half the thickness of the structure, an array of pores resulted at the channel intersections (Fig. 1(c)). Wire electro-discharge machining was used to fabricate the copper structures with the largest channel width (C-0.360-0.7). Fig. 1(d) and (e) presents optical micrographs of lateral and top views, respectively of two channels of structure C-0.065-0.7. Portions of the quartz structure Q-0.200-0.7 are shown in Fig. 1(f) and (g).

3. Experimental setup

The single-layered structures were operated in a thermosyphon loop consisting of an evaporator chamber, connecting tubes and a condenser (Fig. 2). The condenser is placed at a higher elevation than the evaporator to allow liquid return by gravity. The transparent evaporator chamber is made of Plexiglas and has inner dimensions of 40 mm × 40 mm × 30 mm. Four auxiliary foil heaters were placed on the inside lateral walls of the evaporator chamber to maintain the liquid pool at saturation temperature. A dielectric, inert liquid (PF 5060) was used as the working fluid. Its thermophysical properties closely match FC 72 and are available in [10]. The liquid level in the evaporator chamber was main-

Table 1
Geometrical parameters of the enhanced structures

Structure identification[a]	Channel width W_t (mm)	Channel pitch P_t (mm)	Channel depth H_t (mm)	Increase in wetted area (A_w/A)	Fraction of base area in contact with the top cover (A_c/A)
C-0.065-0.70	0.065	0.70	0.6	9.1	0.92
C-0.085-0.70	0.085	0.70	0.6	9.2	0.89
C-0.105-0.70	0.105	0.70	0.6	9.3	0.86
C-0.360-0.70	0.360	0.70	0.6	9.6	0.52
Q-0.065-0.70	0.065	0.70	0.6	9.1	0.92
Q-0.105-0.70	0.105	0.70	0.6	9.3	0.86
Q-0.200-0.70	0.200	0.70	0.6	9.5	0.74
Q-0.250-0.70	0.250	0.70	0.6	9.6	0.68

[a] C denotes copper and Q quartz.

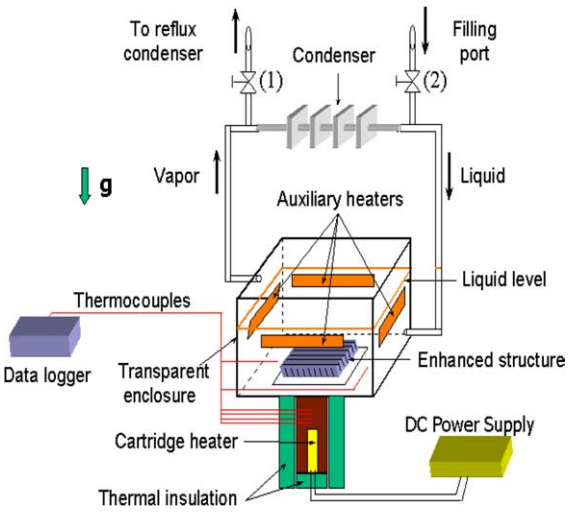

Fig. 2. Schematic of the thermosyphon loop.

tained at 20 mm above the top surface of the structure under un-powered conditions. The system pressure was set at 1 atm in all the experiments by keeping the valve (1) open and valve (2) closed. The dissolved gas content (by volume) was measured before and after each experimental run with a Seaton-Wilson AD-4000 Aire-ometer. The content before charging the system (from the bottle) was 50%, decreasing to 40% after one hour of vigorous boiling and going up to 46% after cooling down (at the beginning of the run).

A plate fin condenser (11 fins) was employed for heat rejection to the ambient. A reflux condenser was placed at a higher elevation in order to trap any escaping vapor. The copper structures were attached to the heating surface using 63Sn 37Pb solder alloy. The thickness of the solder layer was ~50 μm. The thin solder layer provided a strong mechanical bond with a low thermal contact resistance. The quartz structures were bonded to the heating surface with high thermal conductivity silver-filled epoxy. A square (10 mm × 10 mm) quartz plate, 1 mm thick, was attached with adhesive silicone RTV to the enhanced structures to simulate the top-covered case. An Omega cartridge heater embedded in a copper rod with square cross-section (9 mm × 9 mm) was used to provide heat to the structure. To firmly fit the heater into the cavity within the rod, a high temperature, high thermal conductivity paste (Omegatherm® '201', $k_{\text{eff}} = 2.31$ W/m K) was employed. In order to minimize the heat losses, the copper rod was peripherally surrounded with a glass sheath. Thermal insulation and plexiglass provided additional insulation. At the end of the rod four copper-constantan sheathed thermocouples (0.127 mm diameter) were embedded, starting from 4 mm below the enhanced structure. The thermocouples were used to calculate the surface temperature (by extrapolation) and the heat flux at the base of the enhanced structure, assuming one-dimensional heat conduction. The temperature of the liquid pool was monitored using two copper-constantan thermocouples (0.128 mm diameter). All temperatures were measured using an automated data acquisition system (Agilent Inc.).

A regulated DC power supply (0–100 V, 0–0.5 A) powered the cartridge heater. The auxiliary heaters were supplied with power from a dedicated power supply. A precision resistor ($1 \pm 0.01\ \Omega$) connected in series with the power supply served to measure the current. The power dissipation from the heater was determined based on the voltage drop across it and the circuit current.

4. Experimental procedure

The working fluid was maintained at saturation (~56 °C at 1 atm) throughout the experiments. For heat inputs $q > 5$ W (heat flux 4.8 W/cm^2) through the copper rod saturated conditions existed. For lower heat inputs the auxiliary heaters were employed in conjunction with the main heater to maintain saturation conditions throughout the run. A degassing operation preceded every run. The system was kept at atmospheric pressure, while an electrical power input of ~10 W was applied via the cartridge heater. The liquid was boiled vigorously for about one hour, and then allowed to cool down until it reached room temperature. This procedure ensured that the dissolved gas concentration was around 46% (by volume) at the beginning of every run. A real-time air content measurement of the liquid pool near the enhanced structure was not performed. However, the air content is believed to be less than 1% by volume based on Danielson et al. [11].

The electrical power to the cartridge heater was provided in incremented or decremented steps. The power steps were 0.5 W until 2 W, and 1 W from 2 W to 11 W. The six temperatures were monitored continuously, with readings taken after a nominally steady-state was reached. After reaching steady-state, temperatures were recorded for 35 min and mean values were calculated. These values were subsequently used to calculate the surface temperature and the heat input. The heat loss (defined as the difference between the electrical power input and the heat input) was always within 15% (with over 90% of the data within 10%). The heat flux was calculated using the projected surface area (1 cm^2). The experiments were performed for power inputs resulting in a maximum temperature at the base of the enhanced structure of 85 °C. This simulates conditions of interest in electronics cooling.

A high-speed CCD camera (Phantom) was used for visualization. The maximum frame rate is 1000 frames per second at full resolution (512 × 512 pixels). With a

reduction in the field of view, higher frame rates can be achieved. The maximum frame rate used in this study was 2100/s. A zoom lens (Navitar 12× Zoom) attached to the camera through an adapter (Navitar 0.67×) was used to magnify the area of interest and work at close distances to the enhanced structure. The lens is capable of a variable magnification of 1–12 times the original size of the object. A 150 W fiber optic light source (Moritex) was used for providing light to the structure. Movies and still pictures were taken from the top and sides of the structures. The movies were played back at slower speed. From the movies selected frames (single pictures) were also extracted.

The thermocouples and the data acquisition system were calibrated against a precision mercury thermometer at ice point to an uncertainty of 0.1 K. The precision resistor employed for current measurement was accurate to 1%. The voltage measurement uncertainty was specified by the instrument manufacturer as being 0.045% of the reading. The uncertainty in the channel width (5 μm) was due to the uneven width with the depth. The resulting maximum uncertainty in the heat flux was ±20% at low heat fluxes (with over 85% of the data within ±10%). The uncertainty in the wall superheat values was ±0.2 K.

5. Boiling heat transfer performance

The boiling curves obtained for copper structures under saturated condition are presented in Fig. 3. By completely covering the top surface of the structures, the performance decreases considerably in comparison to the open top case. The maximum heat flux attainable (with the wall temperature below 85 °C) was 10.8 W/cm^2 with the structure C-0.105-0.7 and 9.1 W/cm^2 with the structure C-0.360-0.7. A remarkable fact from Fig. 3 is that the copper structures perform nearly similarly, for each channel width. The resulting boiling curves are almost linear (in a log–log plot), indicating the presence of a single boiling regime throughout the range of the investigated heat fluxes. Also plotted in Fig. 3 is the boiling curve obtained with a plain unconfined sample. Within a heat flux range of 1 W/cm^2 < q'' < 4 W/cm^2 the top-insulated enhanced structures show a performance superior to the plain structures with the top open. This behavior is attributable to the prevalence of latent heat transport at low heat fluxes. The enhanced structures have a considerably larger surface area available for heat transfer (see Table 1) and therefore can dissipate more heat at the same wall superheat (through the internal evaporation process). As the heat flux increases, the external convection becomes dominant and the plain surface open to the liquid pool performs better.

Fig. 1(b) represents the top surface of the heater to which the structure in Fig. 1(a) is attached. The black rectangles represent the portions of the heater surface in contact with the fluid, while the white regions represent the portions covered by the structure. The fraction of the heater base surface area on which boiling may occur is therefore $A_b = N \cdot L \cdot W_t$, where N is the number of channels and L is the overall length of the structure. For a constant channel pitch, this area increases with the increase in channel width. The fraction of the base area available for conduction is $A_c = A - A_b$, where A is the base surface area of the heater top. For a smaller channel width or a larger channel pitch, more of the heat leaves the heating surface by conduction. The fraction of bottom surface area exposed to conduction ranges from 50% to 90% (see Table 1).

From the heat transfer data obtained with quartz structures (plotted in Fig. 4) some remarks can be made. The thermal performance is expected to increase with the increase in A_b. However, the heat transfer data presented in Fig. 4 indicate that the quartz structures per-

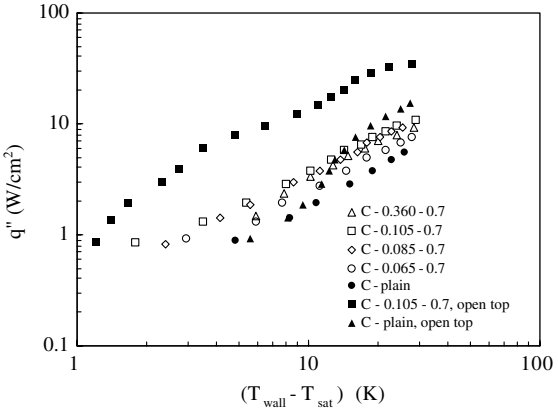

Fig. 3. Boiling curves at saturation for copper structures.

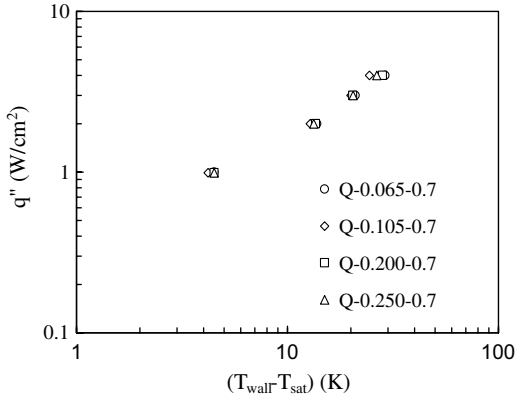

Fig. 4. Boiling curves at saturation for quartz structures.

form similarly at all heat inputs (it is assumed that the thermal contact resistance of the bonding epoxy layer is similar since an identical procedure for attachment is employed for all samples). The conclusion that can be drawn is that the area participating in heat transfer is much less than the channels bottom area A_b. This can be explained by the fact that the vapor slugs seen in the bottom channels form an insulating vapor layer close to the heat transfer surface. Heat transfer, therefore, occurs only through the liquid menisci held in the corners. The area occupied by these menisci is similar for all the structures tested, hence the similar performance. It is believed that increase in performance may be achieved by decreasing the channel pitch and thereby increasing the number of menisci.

For an open top configuration, the conducted fraction of the heat leaves the structure by external convection. This fraction of the heat transfer was found [1] to account for only 10% at a heat flux of 0.1 W/cm^2 and for 70% at a heat flux of 2 W/cm^2. Thus for the range of heat fluxes of interest in electronics cooling, the majority of heat leaves by external convection. By completely covering the top of the structure the decrease in performance is therefore expected, particularly at higher heat fluxes.

The boiling initiation is sometimes explosive and accompanied by a significant and rapid temperature drop. Marto and Lepere [12] noticed a similar explosive initiation for a High-Flux surface. Fig. 5(a) presents a temperature record for structure C-0.105-0.7 capturing the heat-up process and the start of boiling. The temperature is measured at a location below the structure bottom surface. The heat flux is stepped up at time $t = 20$ s to $q'' = 0.85$ W/cm^2 from the previous power level. Initially, the temperature increases without vapor bubbles being generated. As can be seen in Fig. 5(a) at time mark $t = 283$ s the boiling started from top channels. Subsequent activation occurred at $t = 353$ s. The arrows on the graph indicate these moments. Sudden and large drops in surface temperature accompany the boiling incipience. The steady-state zone of the measured temperature trace, which is considered to start at $t = 400$ s, is shown on Fig. 5(b). The surface temperature oscillations with time under nominally steady conditions are believed to be the effect of the transient bubble forming-releasing process inside the structure.

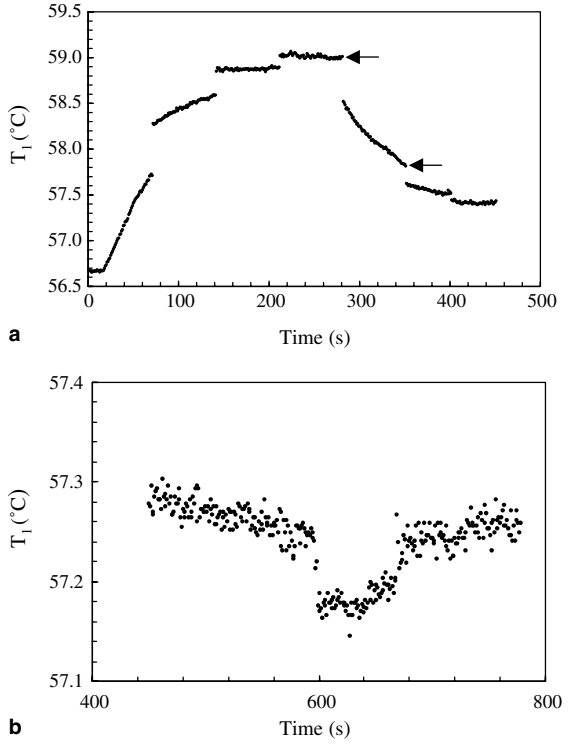

Fig. 5. Wall temperature variation (structure C-0.105-0.7, $q'' = 0.85$ W/cm^2): (a) temperature trace capturing pre-boiling and boiling inception and (b) steady-state zone of the temperature trace.

6. Visualizations

In order to better understand the boiling phenomena from the top-covered enhanced structures, high-speed visualizations were performed for both copper and quartz structures. In both cases, a quartz plate covering the top of the structures permitted visualization of liquid–vapor conditions inside the enhanced structure. The visualizations were performed from the top and lateral positions shown in Fig. 1(a). The results of the photographic observations are presented in detail in the following sections.

6.1. Copper structures

For the opaque copper structures, visualizations can provide information only around the exterior envelope. Visualizations from the sides were performed for structures C-0.065-0.7, C-0.105-0.7 and C-0.360-0.7. The power input was applied in incrementing or decrementing steps. Upon addition of heat, vapor starts to form at random nucleation sites inside the structure and, due to buoyancy, accumulates in the top channels. The vapor formed inside the bottom channels migrates to the top channels through the pores. Due to the constraint exercised by the solid parts of the enhanced structure, the vapor bubbles deform and take the shape of slugs. In general, the significant bubble expulsion process initiates from the top channels. Typical sequences of boiling from structure C-0.065-0.7 are shown in Fig. 6. The frames show the top channels row and were taken under

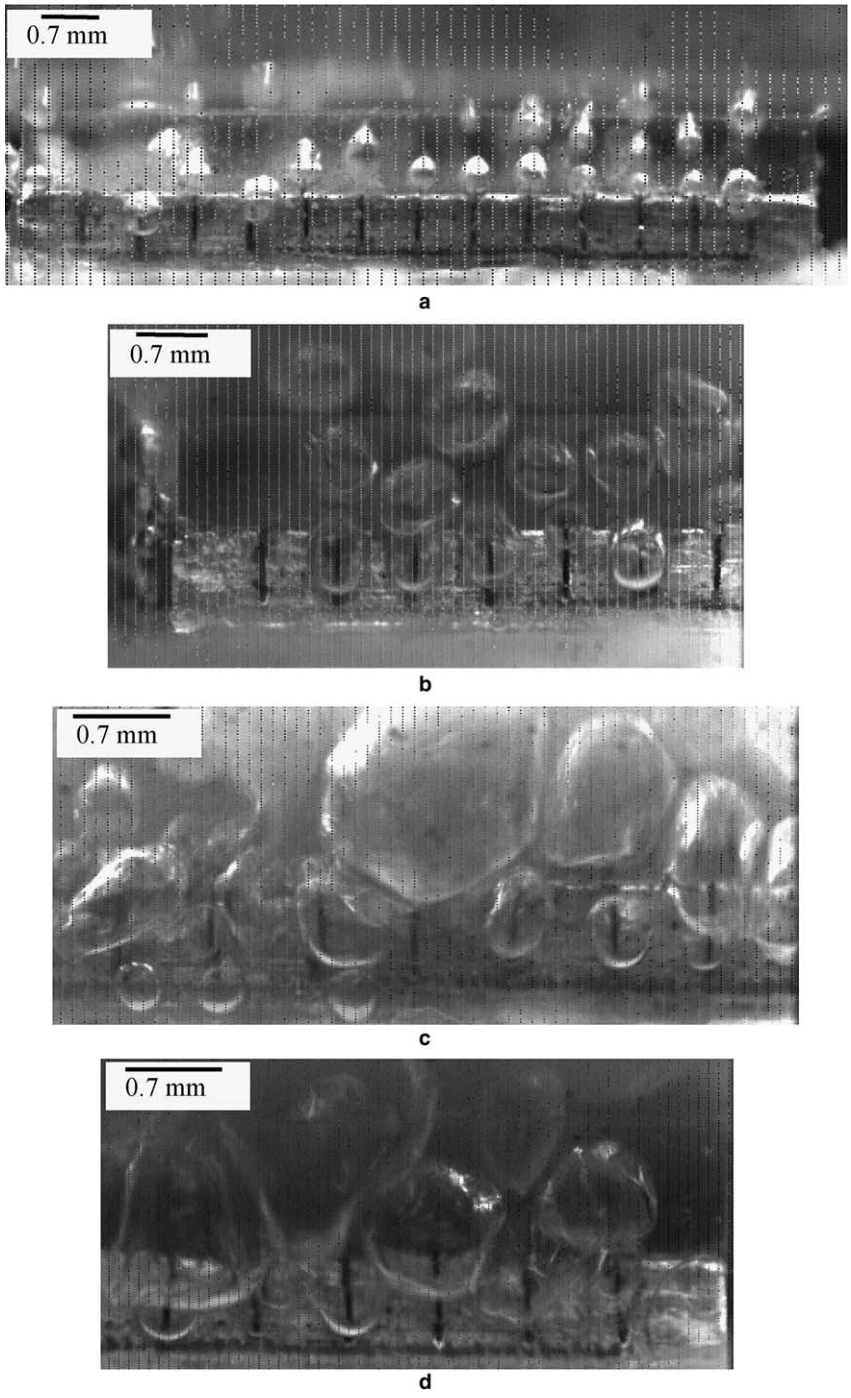

Fig. 6. Lateral view of boiling from structure C-0.065-0.7, top channels: (a) spherical bubbles are emitted, $q'' = 0.8$ W/cm^2; (b) larger bubbles are emitted, $q'' = 1.8$ W/cm^2; (c) big, elongated bubbles are emitted, $q'' = 5.8$ W/cm^2 and (d) vapor bubbles coalesce laterally, $q'' = 6.8$ W/cm^2.

decreasing heat flux conditions. At the lowest heat flux tested ($q'' = 0.35$ W/cm^2) a few active sites were present. The vapor escaped mainly from the upper ends of the top channels in the shape of small, spherical bubbles. The bubbles maintain their individuality during the release process. At higher heat fluxes, more top channels

become active (Fig. 6(a)). The bubble departure diameter increases, bubbles becoming elongated. Fig. 6(b) at a heat flux $q'' = 1.8$ W/cm^2 shows an increase in the bubble departure diameter. However, the bubbles maintain their individuality. These are emitted from all the channel openings, indicating the extent of the vapor regions in the top channels. Bubbles ejected through the end of the channels act as little pumps allowing the pool liquid to enter the structure. The shape and volume of emitted bubbles change with the heat flux. Large, elongated bubbles are being laterally expelled with a high frequency for heat fluxes in excess of 5 W/cm^2 (Fig. 6(c)). Lateral coalescence of bubbles also occurs for heat fluxes in this range. At the highest heat flux

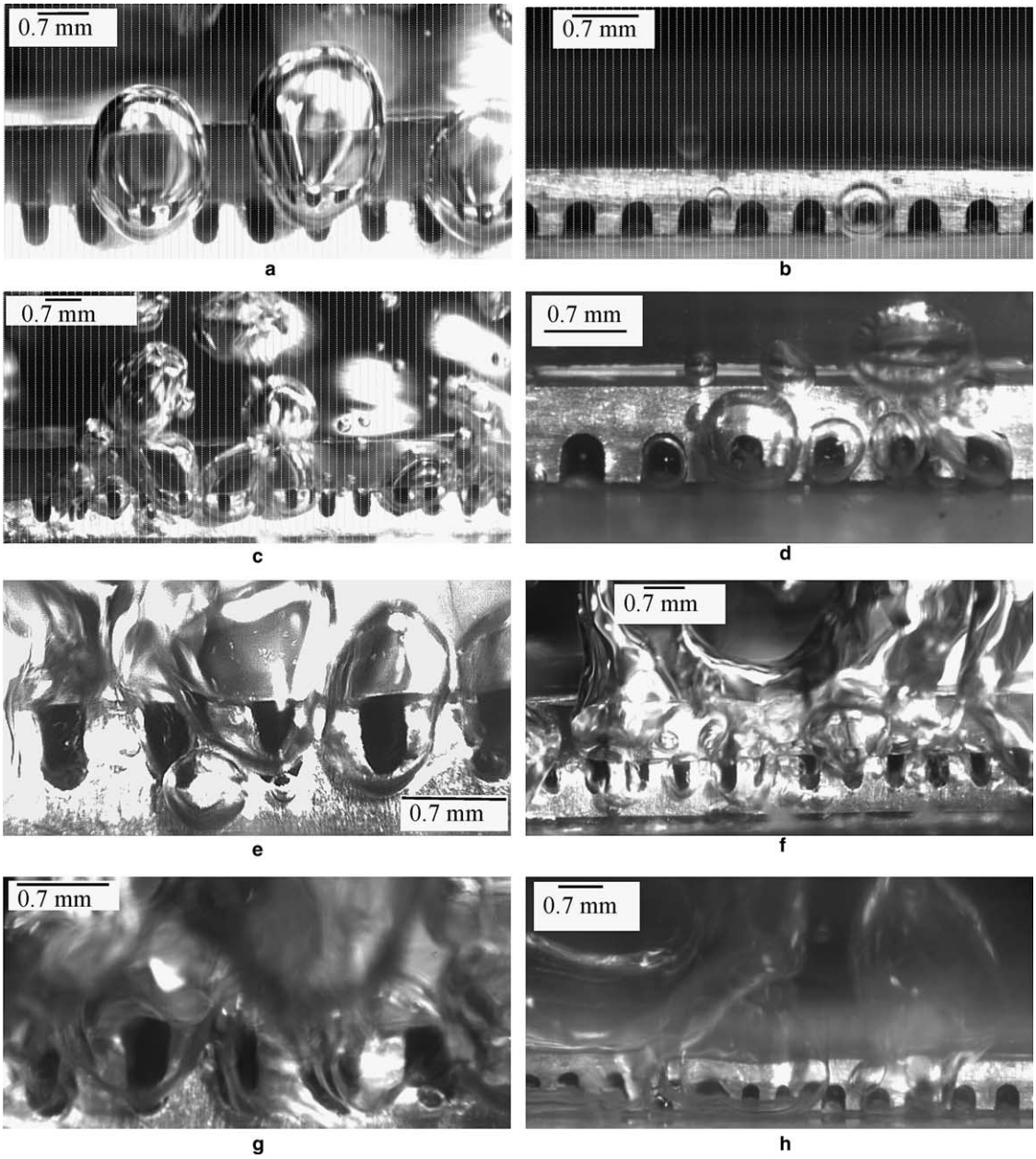

Fig. 7. Lateral view of boiling from structure C-0.360-0.7: (a) single bubble expulsion, top channels, $q'' = 1.4$ W/cm^2; (b) single bubble expulsion, bottom channels, $q'' = 1.4$ W/cm^2; (c) more top channels activate, $q'' = 3.3$ W/cm^2; (d) more bottom channels activate, $q'' = 3.3$ W/cm^2; (e) lateral coalescence, top channels, $q'' = 6$ W/cm^2; (f) lateral coalescence, top channels, lower magnification, $q'' = 6$ W/cm^2; (g) vapor mushrooms, top channels, $q'' = 7.8$ W/cm^2 and (h) vapor mushrooms, bottom channels, $q'' = 7.8$ W/cm^2.

tested, all top and the majority of bottom channels were active Vapor agglomerates laterally in large formations (Fig. 6(d)).

Fig. 7 presents boiling visualizations for the largest width structure (C-0.360-0.7), with increasing heat flux. Boiling started predominantly from the top channels (Fig. 7(a)) at the lowest heat flux tested ($q'' = 1.4$ W/cm^2). When a nucleation site is close to a bottom channel's end, vapor is seen exiting from the bottom (Fig. 7(b)). A nucleation site other than channel ends can also be observed in Fig. 7(b). With the increase in heat flux the number of active top (Fig. 7(c)) and bottom (Fig. 7(d)) channels increases. At even higher heat fluxes, lateral coalescence of bubbles occurs (Fig. 7(e)–(g)). Vapor agglomerates with a mushroom—like shape vertically (Fig. 7(h)) at the highest heat flux ($q'' = 7.8$ W/cm^2).

6.2. Quartz structures

A clearer image of the two-phase phenomena occurring inside the enhanced structure can be obtained through visualizations performed with structures made of transparent materials. For the present study, the material of choice was quartz. Table 1 summarizes the geometrical dimensions of the quartz structures employed in the current study. The parameters investigated were channel width and heat flux. Due to the low thermal conductivity of quartz ($k = 1.2$ W/m K) the top boundary can be considered as nearly adiabatic, with the entire structure being held at saturation temperature (immersed in saturated PF 5060). The heat flux was increased stepwise until the wall temperature reached 85 °C, corresponding to a maximum heat flux of ~4 W/cm^2. The observed phenomena are graphically illustrated in Figs. 8 and 9 as plan views. In the presented figures the top channels are oriented vertically and the bottom channels horizontally.

Fig. 8 presents pictures taken with increasing heat flux during boiling from structure Q-0.105-0.7. Prior to the heat addition, small portions of vapor were observed in the bottom channels (Fig. 8(a)). As the heat was added, extended vapor slugs (shown as black in accompanying cartoons) could be seen forming in the bottom and top channels (Fig. 8(b)). The slugs exhibit an oscillatory motion; especially those formed in the top chan-

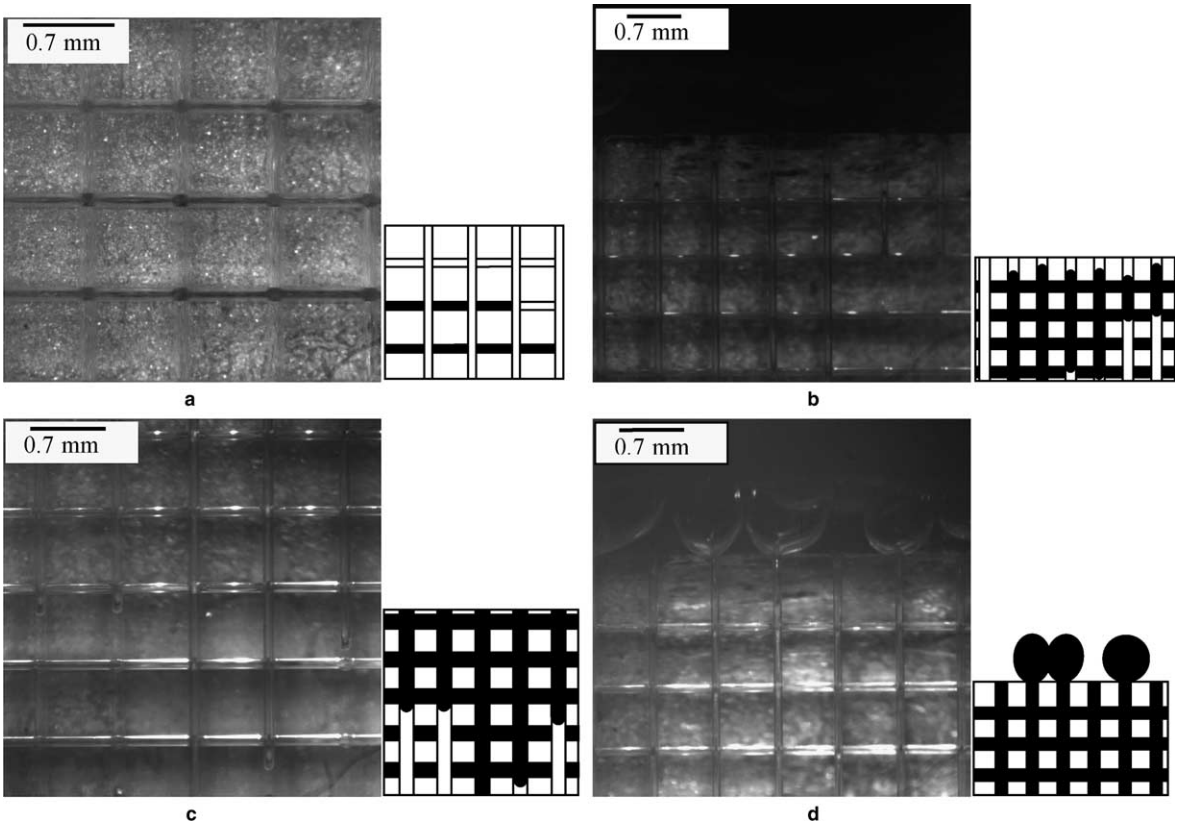

Fig. 8. Boiling from structure Q-0.105-0.7: (a) unheated state, $q'' = 0$ W/cm^2; (b) vapor slugs in the top and bottom channels, $q'' = 0.8$ W/cm^2; (c) liquid plugs in the top channels, $q'' = 1.8$ W/cm^2 and (d) intensified bubble expulsion, $q'' = 3.8$ W/cm^2.

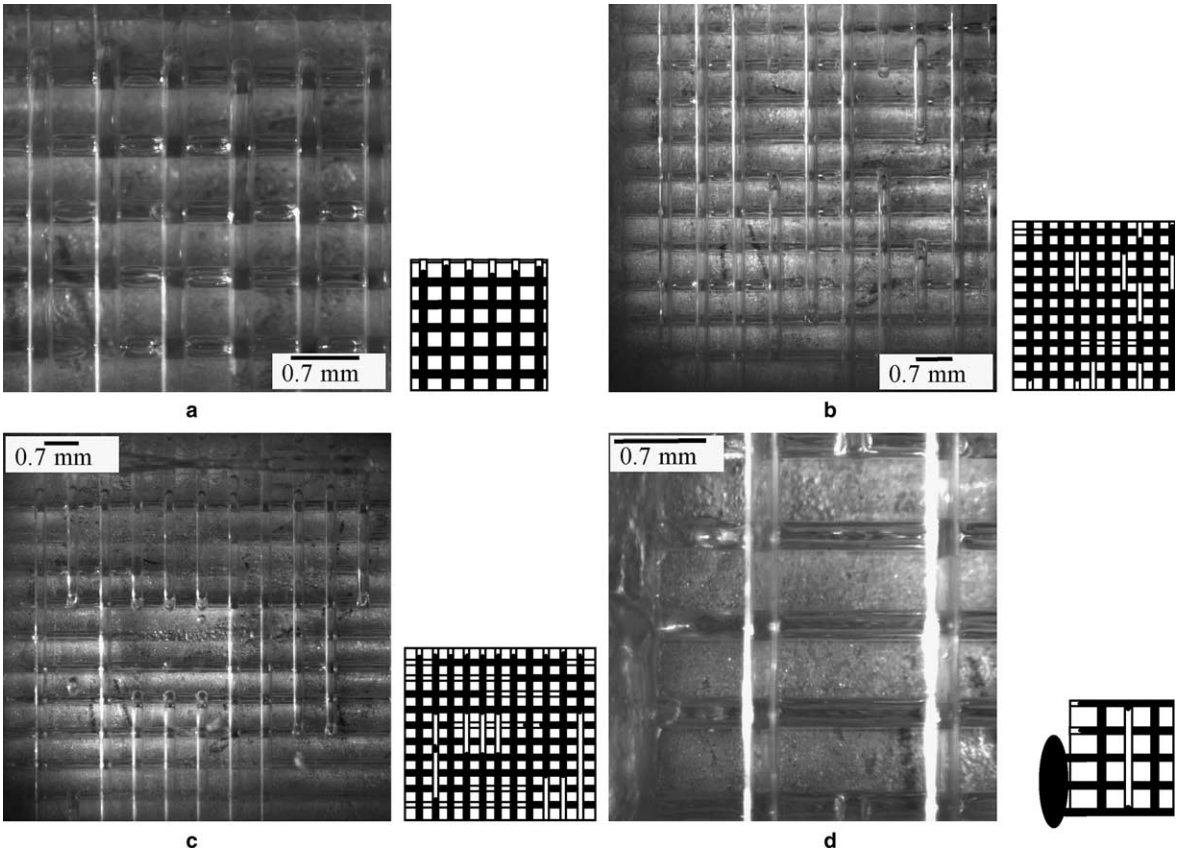

Fig. 9. Boiling from structure Q-0.250-0.7: (a) vapor slugs form at lowest heat flux, $q'' = 0.8\ \mathrm{W/cm^2}$; (b) some vapor slugs become discontinuous, $q'' = 2.8\ \mathrm{W/cm^2}$; (c) liquid plugs in top channels, $q'' = 3.8\ \mathrm{W/cm^2}$ and (d) magnified view of a liquid plug, $q'' = 3.8\ \mathrm{W/cm^2}$.

nels; when a vapor slug reaches the end of a channel, bubbles are expelled in the surrounding liquid pool. Upon further increase of heat flux, the bubble emission intensifies, as more channels become active. Due to the pumping action exercised by the bubbles, liquid plugs are observed forming in the top channels (Fig. 8(c)). At the highest heat flux tested ($q'' = 3.8\ \mathrm{W/cm^2}$) almost all channels expel vapor bubbles (Fig. 8(d)) and liquid plugs occupy portions of the top channels.

Characteristics of boiling pertaining to structure Q-0.250-0.7 are presented in Fig. 9. The pictures are selected from movies made at steady-state conditions with increasing heat flux. At low heat fluxes ($q'' < 1.5\ \mathrm{W/cm^2}$) the majority of top and bottom channels are already filled with vapor slugs (Fig. 9(a)). The vapor slugs show an oscillatory move towards the edges of the structure. There is no lateral vapor release. With increase in the heat flux, the oscillations intensify and vapor is expelled from the sides. Some of the vapor slugs present in the top channels display fragmentation (Fig. 9(b)). Due to the pumping action of the departing bubbles, liquid from the outside pool enters the channels forming plugs. These liquid regions can be clearly seen on central parts of some top channels (Fig. 9(c), $q'' = 3.8\ \mathrm{W/cm^2}$)). Fig. 9(d) (taken at the highest heat flux ($q'' = 3.8\ \mathrm{W/cm^2}$)) presents a magnified view of a region of the structure near the edge. Vapor slugs can be seen in the bottom channels with thin liquid films existing between vapor and walls. In one of the top channels a discontinuity in the vapor slug (filled by a liquid plug) can be observed.

Summarizing, the following events were commonly observed for the channel widths investigated:

(a) After degassing and cool off, small portions of gas were seen in the bottom channels. This can be due to air entrapment during charging.
(b) Vapor formation started at $0.8\ \mathrm{W/cm^2}$ from nucleation sites located on the heated surface (bottom channels). The produced vapor migrated to the top channels through the pores and coalesced forming slugs. Upon reaching steady-state, most of the top channels were filled with vapor. The vapor slugs showed an oscillatory move. At

low heat fluxes the slugs do not reach the sides of the structure, oscillating inside. In some instances the vapor slugs in the top channels expand towards the bottom channels through the pores. The oscillatory move of the vapor slugs is a proof of the intermittent vapor formation, at discrete points on the heating surface. Liquid films were observed in the channels along the edges.

(c) The increase in the heat flux does not change the phenomena described above; it increases the frequency of vapor slug oscillation and the number of expulsion sites. The slugs expand and vapor expulsion activity intensifies from the sides. As a result, lateral coalescence occurs. When a bubble departs, the pressure inside the vapor slug decreases and the slug retreats. At this moment liquid from the pool enters the channel. Sometimes a succession of bubbles is released, followed by a waiting period with no vapor release. When the bubbling activity intensifies, liquid plugs were seen in the top and bottom channels. This phenomenon happens at heat fluxes $q'' \geqslant 2$ W/cm^2.

6.3. Comparison between copper and quartz structures

For the same geometry, along with the expected decrease in performance indicated by the boiling curves, several dissimilarities between boiling from copper and quartz structures are present. At the same heat flux, more nucleation sites form on the internal and external surfaces of the copper structures. The formation of extra nucleation sites is driven partly by the larger wall temperature available in the copper case. As a result, the evaporation process is intensified. Vapor is released in the form of bubbles having significantly different departure diameters (Fig. 7(c) and (d)).

Despite the large difference in thermal conductivity between copper and quartz, it is believed that the visualizations employing transparent structures capture the essential characteristics of boiling under complete confinement. The oscillatory movement of the vapor slugs, vapor expulsion followed by slug retreat and liquid entering the channels, as well as first activation of top channels are phenomena observed in the visualizations experiments with both types of structures.

7. Conclusions

The present study investigates the nucleate pool boiling from enhanced structures under total confinement. Through heat transfer measurements and high-speed visualization the underlying phenomena are illuminated. The study establishes the oscillatory move of the vapor/liquid interfaces as the main characteristic of the liquid/vapor dynamics inside the enhanced structure, regardless of geometric parameters. This confirms the dynamic nature of the boiling process. Additionally, the following conclusions are drawn from the study:

1. The heat transfer performance of the enhanced structures with insulated top decreases significantly in comparison to the open top situation. However, there is a certain range of heat fluxes (1 W/cm^2 $< q'' <$ 4 W/cm^2) for which the top-covered structure outperforms a plain structure with the top open.
2. The heat transfer performance of the enhanced structure with insulated top has only a marginal dependence on the channel width. It is hypothesized that the channel pitch may have a bigger influence through the number of menisci created inside the channels.
3. The boiling curves obtained with enhanced structures completely confined show no change in slope over the tested heat flux range; however, the visualizations indicate the presence of two boiling regimes: slug predominance regime and slugs and plugs regime.
4. The internal evaporation process is an important heat transfer mechanism; its contribution to the total dissipated heat is significant, especially at low heat fluxes.
5. Vapor slugs exist in the top and bottom channels even for the lowest heat fluxes and exhibit an oscillatory movement. This is believed to be an effect of the transient nature of internal evaporation.

Acknowledgements

This work was supported by Semiconductor Research Corporation contract 649.001 and Defense Advanced Research Projects Agency HERETIC Program under contract N00164-99-C-0039. The authors would like to acknowledge Professor Sushil Bhavnani from Auburn University for facilitating the air concentration measurement.

References

[1] W. Nakayama, T. Daikoku, H. Kuwahara, T. Nakajima, Dynamic model of enhanced boiling heat transfer on porous surfaces, part I: experimental investigation, J. Heat Transfer 102 (1980) 445–450.

[2] W. Nakayama, T. Daikoku, H. Kuwahara, T. Nakajima, Dynamic model of enhanced boiling heat transfer on porous surfaces, part II: analytical modeling, J. Heat Transfer 102 (1980) 451–456.

[3] W. Nakayama, T. Daikoku, T. Nakajima, Effects of pore diameters and system pressure on saturated pool nucleate boiling heat transfer from porous surfaces, J. Heat Transfer 104 (1982) 451–456.

[4] J. Arshad, J.R. Thome, Enhanced boiling surfaces: heat transfer mechanism mixture boiling, in: Y. Mori, W.-J. Yang (Eds.), Proceedings/ASME-JSME Thermal Engineering Joint Conference, Honolulu, Hawaii, 1983, vol. 1, pp. 191–197.

[5] L.-H. Chien, R.L. Webb, Visualization of pool boiling on enhanced surfaces, Exper. Therm. Fluid Sci. 16 (1998) 332–341.

[6] W. Nakayama, T. Nakajima, S. Ohashi, H. Kuwahara, Modeling of temperature transient of microporous studs in boiling dielectric fluid after stepwise power application, in: R.K. Shah (Ed.), Proceedings of the National Heat Transfer Conference, Philadelphia, PA, vol. 111, 1989, pp. 17–23.

[7] C.-D. Ghiu, Y.K. Joshi, W. Nakayama, Visualization study of pool boiling from transparent enhanced structures, in: T.L. Bergman, C.B. Panchal (Eds), Proceedings of the 2001 National Heat Transfer Conference, Anaheim, CA, 2001, vol. 1, pp. 697–704.

[8] K. Banerjee, S.J. Souri, P. Kapur, K.C. Saraswat, 3-D ICs: a novel chip design for improving deep-submicrometer interconnect performance and systems-on-chip integration, Proc. of IEEE 89 (2001) 602–603.

[9] C. Ramaswamy, A compact two-phase thermosyphon employing microfabricated boiling enhancement structures, Ph.D. Thesis, University of Maryland at College Park, MD, 1999.

[10] 3M Company, 1995, Specialty Fluids Newsletter, vol. 1, No. 1.

[11] R.D. Danielson, L. Tousignant, A. Bar-Cohen, Saturated pool boiling characteristics of commercially available perfluorinated inert liquids, in: P.J. Marto, I. Tanasawa (Eds.), Proceedings of 1987 ASME-JSME Thermal Engineering Joint Conference, Honolulu, Hawaii, vol. 3, 1987, pp. 419–430.

[12] P.J. Marto, V.J. Lepere, Pool boiling heat transfer from enhanced surfaces to dielectric fluids, J. Heat Transfer 104 (1982) 292–299.